

Quantitative phosphotyrosine profiling of patient-derived xenografts identifies therapeutic targets in pediatric leukemia

Sibasish Dolai¹, Keith C. S. Sia¹, Alissa K. Robbins¹, Ling Zhong², Sue L. Heatley^{3,4}, Tiffany L. Vincent⁵, Falko Hochgräfe⁶, Rosemary Sutton¹, Raushan T. Kurmasheva⁷, Tamas Revesz^{8,9}, Deborah L. White^{3,4,8}, Peter J. Houghton⁷, Malcolm A. Smith¹⁰, David T. Teachey⁵, Roger J. Daly¹¹, Mark J. Raftery², Richard B. Lock¹.

¹Children's Cancer Institute, Lowy Cancer Research Centre, UNSW Australia, Sydney, NSW, Australia.

²Bioanalytical Mass Spectrometry Facility, Mark Wainwright Analytical Centre, UNSW Australia, Sydney, NSW, Australia.

³South Australian Health and Medical Research Institute (SAHMRI), Adelaide, SA, Australia.

⁴Discipline of Medicine, University of Adelaide, Adelaide, SA, Australia

⁵Children's Hospital of Philadelphia, Philadelphia, PA, USA.

⁶Competence Centre – Functional Genomics, Junior Research Group Pathoproteomics, University of Greifswald, Germany.

⁷Greehey Children's Cancer Research Institute, UT Health Science Center, San Antonio, TX, USA.

⁸Discipline of Paediatrics, University of Adelaide, Adelaide, SA, Australia

⁹SA Pathology (at Women's & Children's Hospital), Adelaide, SA, Australia

¹⁰Cancer Therapy Evaluation Program, NCI, Bethesda, MD, USA.

¹¹Department of Biochemistry and Molecular Biology, School of Biomedical Sciences, Monash University, Melbourne, VIC, Australia.

Running title: Quantitative phosphotyrosine profiling in xenograft models of leukemia

Keywords: leukemia, tyrosine kinases, phosphotyrosine profiling, proteomics, mass spectrometry

Financial Support: This research was funded by Project Grant 1024232 from the Australian National Health and Medical Research Council. R.B.L. is supported by a Senior Research Fellowship (1059804) from the Australian National Health and Medical Research Council.

Correspondence:

Richard B Lock, PhD, Children's Cancer Institute,

PO Box 81, Sydney, NSW 2031, Australia; Phone, +61-2-9385-2513; FAX, +61-2-9662-6584;

Email: - RLock@ccia.org.au

Conflict of Interest Disclosure: The authors declare no conflict of interest.

Text word count: 4692

Abstract word count: 194

Figures and table: 7

References: 50

ABSTRACT

Activating mutations in tyrosine kinases (TKs) drive pediatric high-risk acute lymphoblastic leukemia (ALL) and confer resistance to standard chemotherapy. Therefore, there is urgent need to characterize dysregulated TK signaling axes in patients with ALL and identify actionable kinase targets for the development of therapeutic strategies. Here, we present the first study to quantitatively profile TK activity in xenografted patient biopsies of high-risk pediatric ALL. We integrated a quantitative phosphotyrosine profiling method with 'spike-in' stable isotope labeling with amino acids in cell culture (SILAC) and quantified 1394 class I phosphorylation sites in 16 ALL xenografts. Moreover, hierarchical clustering of phosphotyrosine sites could accurately classify these leukemias into either B or T-cell lineages with the high-risk early T-cell precursor (ETP) and Ph-like ALL clustering as a distinct group. Furthermore, we validated this approach by using specific kinase pathway inhibitors to perturb ABL1, FLT3, and JAK TK signaling in four xenografted patient samples. By quantitatively assessing the tyrosine phosphorylation status of activated kinases in xenograft models of ALL, we were able to identify and validate clinically relevant targets. Therefore, this study highlights the application and potential of phosphotyrosine profiling for identifying clinically relevant kinase targets in leukemia.

INTRODUCTION

Acute lymphoblastic leukemia (ALL) is the commonest cancer in childhood and adolescent age groups, accounting for a third of all pediatric malignancies and 80% of childhood leukemia (1,2). The disease results from a clonal proliferation of malignant, immature white blood cells of B- and T-cell lineages in the bone marrow. The B cell precursor (BCP) - and T-ALL are further divided into a number of subtypes based on clinical features, chromosomal translocations, and genetic characteristics (3). Despite an overall survival rate approaching 90%, the heterogeneous nature of ALL confers a differential response to treatment for the diverse patient groups (4). Given this heterogeneity in prognosis, modern therapeutic approaches seek to modify treatment regimens based on a patient's risk of relapse at diagnosis using clinical, cytogenetic and biological criteria, in risk-adapted therapy (5,6). More recently, attempts have been made to improve risk stratification by classifying these high-risk patients into distinct subtypes at a molecular level, via gene expression analysis and immunophenotyping (7,8). Whole genome and transcriptome sequencing of certain high-risk patient subsets such as early T-cell precursor ALL (ETP-ALL) (9,10) and Philadelphia Chromosome-like (Ph-like) (11,12) ALL have also revealed several activating gene fusions, alterations and mutations that could result in constitutively activated tyrosine kinases (TKs). This further leads to unconstrained phosphorylation of downstream substrates by TKs, impacting several key signaling pathways and resulting in increased cell survival and proliferation.

Recent advances in mass-spectrometry (MS) and the use of anti-phosphotyrosine antibodies for enrichment of tyrosine phosphorylated peptides have greatly facilitated characterization of kinase signaling networks and identified several activated TKs and their phosphorylated substrates in cancer cells (13-15). Further, quantitative tools such as stable isotope labelling by amino acids in cell culture (SILAC) have also been efficiently integrated into this phosphoproteomic workflow to globally map and quantify changes in phosphorylation events (16,17). Using such an approach, activated oncogenic kinases were identified in non-small cell lung cancer patient samples (15). Phosphotyrosine profiling also revealed specific signaling networks in basal breast cancer cells and highlighted multiple kinases and substrates for therapeutic evaluation (18). These studies also indicate that patient stratification is feasible based on activated kinase profiles, which could suggest specific kinase targeted drugs to be used either alone or in combination with established

chemotherapeutics. While this quantitative approach has been successfully extended to patient samples in solid tumors, studies in hematologic disorders have been confined to cell line models.

In this study, we have used an MS-based phosphotyrosine profiling approach to characterize activated TK signaling in patient derived xenografts (PDXs) of high-risk pediatric ALL patients. Integrating a 'spike-in' SILAC approach, we mapped close to 1900 class I phosphosites with >0.75 localization probability and 99% confidence in 16 PDXs, of which 1394 tyrosine phosphorylated sites had a heavy SILAC partner that allowed quantification. In particular, individual PDXs with ABL1, FLT3 and JAK mutations with aberrant kinase signaling were targeted with commercially available TK inhibitors (TKIs) both *in vitro* and *in vivo*. Aberrant ABL1 kinase signaling observed in a Ph⁺-ALL and a PDX with high phospho-ABL1 (harboring a *NUP214-ABL1* translocation) indicated dasatinib treatment and a significant delay in disease progression was achieved in these PDXs. Similarly, the uniquely activated FLT3 in one PDX correlated with an objective response to the multi-kinase inhibitor sunitinib. Thus, this study demonstrates an important step forward in the pre-clinical utility of an unbiased and quantitative tool to identify aberrant TK signaling in high-risk ALL PDXs and highlights its potential to identify tractable drug targets.

METHODS

Patient derived xenografts and sample preparation

All PDX studies had received prior approval from the respective institute's Human Research Ethics Committees and Animal Care and Ethics Committees. Continuous xenografts from childhood ALL biopsies (demographics detailed in Table 1) were established in immune-deficient mice as described previously (19,20). Spleens with >95% infiltration of human leukemic cells were harvested and mononuclear cells were used for sample preparation. Methods for PDX engraftment, *in vivo* drug efficacy and proteomic sample preparation are detailed in Supplementary Materials and Methods.

Cell culture and SILAC labeling

The JURKAT (T-ALL), NALM-6 (BCP-ALL), MUTZ-5 and MCH-CALL-4 (JAK mutated/CRLF2 high BCP-ALL) cell lines were used in this study and had been validated by STR analysis no more than 3 months prior to use. Cells were cultured in RPMI flex media (lacking arginine and lysine) (Invitrogen, Carlsbad, CA) with 10% (JURKAT, NALM-6) or 20% (MUTZ-5 and MCH-CALL-4) dialyzed fetal bovine serum, 10 mM Glutamax and 1% penicillin/streptomycin and supplemented with heavy ($^{13}\text{C}_6$ -lysine and $^{13}\text{C}_6$ and $^{15}\text{N}_4$ -arginine) isotopes (98% purity; Cambridge Isotope Laboratories, Andover, MA). The heavy media were also supplemented with 200 mg/L of *L*-proline to circumvent the arginine to proline conversion, as previously described (4). The cells were cultured for six doubling times to incorporate heavy amino acids into proteins and were monitored by MS. The heavy labeled cells were pervanadate treated and lysed using urea lysis buffer (8 M urea, 2.5 mM sodium pyrophosphate, 1 mM β -glycerol phosphate, 1 mM sodium orthovanadate and 20 mM HEPES, pH 8.0) prior to protein quantification using the bicinchoninic acid (BCA) assay (Thermo Scientific, Waltham, MA). All four heavy labeled cell lysates were mixed in a 1:1:1:1 ratio to generate the internal standard SILAC MIX that was spiked into the PDX samples for immunoaffinity enrichment. The 16 PDXs that were included in this study had four groups of molecularly defined leukemias; B-ALL, T-ALL, ETP-ALL and Ph-like ALL, of which ETP-ALL and Ph-like ALL had JAK mutations. To allow the JAK pathway signaling proteins that are activated in the JAK mutated PDXs to have SILAC labeled partners for quantification, we included 2 JAK

mutated cell lines (MUTZ5 and MHH-CALL4) for SILAC labeling. The inclusion of 2 JAK mutated cell lines with different JAK mutations along with the BCP-ALL and the T-ALL cell lines helped generate a pool of representative labeled peptides from cell lines to complement all the 16 PDXs under investigation.

Phosphopeptide immunoprecipitation

Lysates from the PDX samples were spiked with SILAC MIX and were reduced, alkylated and trypsin digested as previously described (21,22). Purified and lyophilized peptides were immunoenriched using P-Tyr-100 antibody as described previously (14,18,23). Enriched phosphotyrosine peptides were subjected to TiO₂-based phosphopeptide enrichment using TiO₂ microcolumns (GL Sciences, Tokyo, Japan) as described by Larsen et al. (24) following the manufacturer's protocol to facilitate removal of antibody fragments and non-phosphorylated peptides that co-elute in the elution step. Detailed methods of phosphopeptide immunoprecipitation with SILAC spiked PDX samples and TiO₂ microcolumn cleanup are described in Supplementary Materials and Methods.

Mass spectrometry and data analysis

Mass spectra of phosphotyrosine immuno-purified peptides were generated in an Orbitrap Velos (Thermo Electron, Bremen, Germany) mass spectrometer. Raw mass spectrometric files were analyzed in MaxQuant (25) version 1.3.0.5 for feature detection, protein identification, and quantification using the integrated Andromeda search engine for database searching (26). Methods for liquid chromatography, mass-spectrometry, MaxQuant search criteria, protein identification and quantification are detailed in the Supplemental Materials and Methods

In vitro cytotoxicity assays and immunoblotting

PDXs were assessed for single agent kinase inhibitor *in vitro* drug sensitivity by Alamar blue and the dephosphorylation of phosphorylated kinase targets post inhibitor treatment was validated using immunoblotting as detailed in the Supplemental Materials and Methods.

Gene expression analysis

Microarray analysis of gene expression using RNA extracted from patient and xenograft cells was carried out as described in the Supplemental Materials and Methods.

RESULTS

Phosphotyrosine profiling in PDX models of pediatric ALL

To characterize the global tyrosine phosphorylation status in pediatric ALL PDXs we adopted an immunoaffinity profiling of phosphotyrosine peptides protocol as described earlier (14,15,18). Patient demographics of the 16 PDXs, along with their subtype classification and key molecular lesions, are listed in Table 1.

To initially establish the immunoaffinity profiling in PDX models, two T-ALL (ALL-8, ALL-31) and two BCP-ALL (ALL-17, ALL-19) PDXs were selected. Using the phosphotyrosine immunoaffinity profiling method, we identified 540 Class I phosphotyrosine sites along with 61 phosphoserine and 49 phosphothreonine sites (Supplementary Table S1). These sites correlated to 424 phosphoproteins of which 17% were kinases (Supplementary Fig. S1A). This method enabled us to identify phosphorylation on all the key TKs that have been reported in T-cell signaling pathways in the two T-ALL PDXs, ALL-8 and ALL-31 (27). For example, ZAP70 and LCK (Supplementary Fig. S1B) were identified along with other T-cell associated signaling molecules CD3, CD247, LAT, GRAP2 and SH2D2A (highlighted in yellow in Supplementary Table S1). ZAP70 is an essential kinase in T-cell signaling and its phosphorylation is indicative of recruitment of other T-cell signaling proteins (LCK, LAT) (16).

As expected, phosphorylation at the T-cell-specific sites was not observed in the BCP-ALL PDXs, in which the identified phosphotyrosine sites were primarily B-cell signaling molecules. The TKs SYK, BTK and LYN were highly phosphorylated in the BCP-ALL PDXs (Supplementary Fig. S1B and highlighted red Supplementary Table S1). ALL-19 was the only BCP-ALL PDX with markedly elevated tyrosine phosphorylation of ABL1 kinase. We then plotted the combined intensity of all phosphorylated tyrosine sites in a TK against the total intensity of all the identified TKs in that PDX (Supplementary Fig. S1B). The pie charts clearly show the distinction between the T- and BCP-ALL PDXs based on the intensity of TK-specific tyrosine phosphorylated peptides. The phosphotyrosine sites of the TKs identified either in T-ALL or in the BCP-ALL PDXs are listed in Supplementary Table S2.

Quantitative phosphotyrosine profiling

In order to compare phosphotyrosine profiles across multiple PDXs we undertook developing a more quantitative analysis method. The immunoaffinity protocol optimized for the PDX models was combined with a 'spike in' SILAC (21,28) approach to generate a quantitative phosphotyrosine profile of high-risk pediatric ALL. Fig. 1 shows a schematic of the quantitative phosphotyrosine profiling approach in PDX models of ALL. As profiling of phosphotyrosine sites in cellular signaling is compounded with artifacts when clinical sample processing is delayed or when samples are frozen (29), extra care was taken for extraction of proteins under optimal conditions from freshly harvested human mononuclear cells from mice spleens. In fact, we compared phosphotyrosine enrichment of freshly processed ALL-2 PDX cells with that of frozen ALL-2 PDX cells that were stored in liquid nitrogen in a FBS+10% DMSO medium. Both the frozen and fresh ALL-2 PDX samples were the same in all respects (generated from the same patient biopsy and harvested from mice at the same passage number) with freezing being the only variable. As expected the number of class I phosphotyrosine sites were reduced by 80% in frozen samples compared to freshly harvested ALL-2 spleens (Supplementary Fig. S2A). Further, as a novel heterozygous FLT3 mutation (c.1715A>C; p.Y572S) was observed in the ALL-2 PDX, we tracked the tyrosine phosphorylated sites on FLT3. In the fresh ALL-2 samples two autophosphorylated FLT3 sites (Y842 and Y969) were identified compared to only one (Y842) in the frozen ALL-2 samples. Moreover the intensity of the Y842 site was a third in frozen samples compared to freshly lysed samples (Supplementary Fig. S2B). All the PDX samples used in this study were freshly harvested and lysed under optimal conditions using appropriate phosphatase and protease inhibitors.

As all PDX samples were spiked with equal concentration of the heavy labeled internal standard, the light (PDX) to heavy (SILAC) ratio generated for each of the enriched phosphopeptides enabled an accurate indication of their relative abundance. This allowed a direct comparison of phosphopeptide abundance between different ALL PDXs relative to the SILAC standard. To ensure the amount of heavy labeled phosphopeptide enriched during the immunoaffinity process was sufficient to provide quantitative information on the light phosphopeptides enriched from the PDX sample, different ratios of starting material and 'spike in' standard were initially tested (Supplementary Fig. S3) and the optimized 20:1(PDX:SILAC) ratio

was then used to generate quantitative phosphotyrosine profiling data on a panel of 16 PDXs, including 4 BCP-ALL, 5 T-ALL, 4 ETP-ALL and 3 Ph-like ALL (Table 1).

Enriched phosphopeptides from at least two technical replicates for each PDX (up to 4 replicates for some) were identified by mass spectrometry. Using this quantitative phosphotyrosine method we mapped in total 1912 class I phosphosites (1375 phosphotyrosine, 376 phosphoserine and 161 phosphothreonine) with >0.75 localization probability and 99% confidence (Supplementary Table S3). Of these, 1394 class I phosphosites (73%) had a heavy partner intensity that allowed quantification (Supplementary Table S4). The number of phosphosites identified and quantified in each of the PDXs is represented in Supplementary Fig. S4. Marked differences were observed in the number of class I phosphosites that were identified in each of the different subgroups. While the highly aggressive ETP-ALL and the Ph-like ALL PDXs had higher number of phosphosites ranging from 400 to 850, the other T-ALL and BCP-ALL PDXs had phosphosites ranging from 250 to 400 (Supplementary Fig. S4).

Hierarchical clustering based on the average normalized ratios of all quantified phosphotyrosine sites (Supplementary Table S4) for each PDX revealed clustering into two distinct groups broadly based on B and T lineage (Fig. 2A), with the stem cell like ETP-ALL clustering either with the B lineage (ETP-12 and ETP-1) or with the T lineage (ETP-13 and ETP-8). In the BCP-ALL group the Ph⁺-ALL, ALL-4 clustered independently of the remaining PDXs. Notably, segregating the molecularly-defined ETP, Ph-like, and Ph⁺-ALL PDXs and re-clustering them resulted in grouping according to their subtype (Supplementary Fig. S5). Further, the distinct clustering into the B and T lineages was also validated by gene expression profiling. Unsupervised hierarchical clustering of basal gene expression profiles of 14 PDXs revealed 2 broad branches reflecting each leukemia subtype (Supplementary Fig. S6A).

Quantitative analysis of TK phosphotyrosine sites

Unsupervised hierarchical clustering was performed to identify PDX clustering patterns based on the identified phosphotyrosine sites on TKs. As shown in Fig. 2B the 16 PDXs clustered into 2 broad groups, separating the BCP-ALL from the T-ALL and a distinct group consisting of the highly aggressive ETP-ALL and Ph-like ALLs. The only exception was ETP-8, which clustered with the T-

ALLs. Unsupervised hierarchical clustering of TKs by microarray analysis of gene expression in 14 PDXs also showed 2 broad groups, separating the T-ALL PDXs from the BCP-ALL and Ph-like ALLs, with one ETP-ALL clustering each with the T-ALL and BCP-ALL clusters (Supplementary Fig. S6B).

Analysis of individual PDXs revealed that in the Ph⁺-ALL, ALL-4 the TKs ABL1 (Y469, Y393), DDR1 (Y792, Y796) and PTK2B (Y579, Y580) showed the highest levels of tyrosine phosphorylation, along with BTK, CSK, FYN and EPHB4 (Fig. 2B and Supplementary Table S5). Similarly, the receptor TK (RTK) ZAP70 phosphosites (Y493, Y292 and Y248) were uniquely present in the ETP group with Y248 having the highest level of phosphorylation in ETP-12, ETP-13 and ETP-1 (Supplementary Table S5). Y493 and Y292 have previously been reported as autophosphorylation sites responsible for the complete activation of ZAP70 by displacing the activation loop from the catalytic site (30). Furthermore, in the ETP group ETP-8 had the highest levels of phosphorylation of the JAK1 autophosphorylation phosphosites Y1034/35, which could be a post translational effect of the activating JAK1 mutations described by Zhang et al. in ETP-ALL (10).

In the Ph-like ALL group, the TKs with the highest levels of tyrosine phosphorylation included INSR, JAK1, JAK2, LYN, FYN, SYK and LCK (Fig. 2B and Supplementary Table S5). The RTK INSR has previously been reported to be involved in pre-B leukemia (31) and this kinase had the highest level of phosphorylation in this group with phosphorylation at 5 different sites (Y1190, Y1189, Y1185, Y1355 and Y1361). Conversely, Y842 FLT3 was unique to PAMDRM across the entire panel, while the Y570 site in JAK2 and the Y702 site in AXL were unique to PALLSD. PALLSD also had Y209 HCK, Y344 BTK, Y145 DYRK1A and Y188 BLK phosphosites unique to itself. A complete list of all the TK phosphotyrosine sites that were identified in the ETP-ALL, Ph-like and Ph⁺-ALL PDXs is shown in Fig. 2B and Supplementary Table S5.

As anticipated, the highest levels of TK phosphotyrosine sites in T-ALL PDXs included ZAP70, LCK and FYN, with none of these identified in the BCP-ALL PDXs (Fig. 2B). In fact, the Y420 site of FYN that regulates T-cell receptor signaling by autophosphorylation was present at very high levels in all 5 T-ALL PDXs compared with the BCP-ALLs. Within the BCP-ALLs, ALL-19 had the highest level of phosphotyrosine sites on ABL1 (Y393), LYN (Y194, Y193), INSR (Y1189, Y1185)

and JAK2 (Y1007). In particular, the autophosphorylation site Y1007 of JAK2 was uniquely observed in ALL-19, while the RTKs FLT3 and EPHB4 and the non-receptor TK (nRTK) TYK2, were uniquely identified in ALL-2. Both of the identified FLT3 phosphosites in ALL-2 (Y842 and Y969) are key autophosphorylation sites for kinase signaling activation (32). The profound differences in levels of pTyr site phosphorylation of TKs (ABL1, FLT3 and JAK1) and key signaling substrates could not be explained by mere differences in gene expression levels (Supplementary Fig. S7).

Dysregulated phosphotyrosine sites as drug targets

We further investigated altered tyrosine phosphorylation in pediatric ALL PDXs to assess the therapeutic potential of specific TKIs. Immunoblots were performed to validate activated sites and their dephosphorylation upon TKI treatment, and *in vitro* cytotoxicity assays and/or *in vivo* efficacy experiments were performed to determine drug efficacy.

The autophosphorylation site of the ABL1 kinase Y393 was notably upregulated in ALL-4 (Fig. 3A). The upregulation of this site has also been confirmed by others studying BCR-ABL1 signaling in chronic myeloid leukemia (13,23). Imatinib-sensitive tyrosine phosphorylation sites in GAB1, SHC, BCR, ABL and STAT5A were also identified (highlighted in yellow, ALL-4 sheet, Supplementary Table S6). Furthermore, upregulation of tyrosine phosphorylation sites in the SRC kinase family members (SRC, FYN, FGR, LCK, HCK, BLK and LYN) (highlighted in yellow, ALL-4 sheet, Supplementary Table S6), prompted us to test the TKI dasatinib against ALL-4. Exposure of ALL-4 cells to dasatinib resulted in complete dephosphorylation of pCRKL and pSTAT5 (Fig. 3B). The BCP-ALL PDX ALL-19 also exhibited very high intensity of ABL1-pY393, despite the absence of the *BCR-ABL1* translocation (Fig. 3A), and downstream targets are highlighted in yellow, ALL-19 sheet, Supplementary Table S6). Upon dasatinib treatment ALL-19 showed similar dephosphorylation of pCRKL and pSTAT5 as ALL-4 (Fig. 3B), although ALL-4 and ALL-19 exhibited disparate *in vitro* sensitivity to dasatinib (Fig. 3C). ALL-4 and ALL-19 were also evaluated for their *in vivo* sensitivity to dasatinib monotherapy (33). While dasatinib significantly decreased the proportion of both ALL-4 and ALL-19 cells in the murine peripheral blood compared with vehicle-treated control mice (Fig. 3D), the sensitivity of ALL-4 (Complete Response) was greater

than ALL-19 (significant progression delay). Subsequent analysis to investigate the aberrant ABL1 in ALL-19 using RT-PCR of fusion partner panels revealed a rare *NUP214-ABL1* translocation. This translocation in the ALL-19 patient was further confirmed by Sanger sequencing (data not shown).

Phosphorylated FLT3 (Y969, Y842) (Fig. 4A and B) was markedly upregulated only in ALL-2 along with phosphorylation of key downstream tyrosine phosphorylation targets (GAB1, GAB2, STAT5A, STAT3 and PLCG2) (highlighted in ALL-2 sheet, Supplementary Table S6). Exposure of ALL-2 cells to the multi-targeted TKI sunitinib *in vitro* resulted in a marked dephosphorylation of pFLT3 (Fig. 4C). Subsequent exome sequencing of ALL-2 revealed a novel heterozygous mutation in FLT3 (c.1715A>C; p.Y572S). While ALL-2 demonstrated limited *in vitro* sensitivity to sunitinib (Supplementary Fig. S8), it was the only PDX out of 8 tested to achieve an objective response (Complete Response) to sunitinib monotherapy when tested *in vivo* (Fig. 4D) (34).

The unbiased quantitative phosphotyrosine profiling of high-risk pediatric ALL PDXs also revealed elevated levels of phosphorylation of JAK1 phosphosites in all of the ETP-ALL PDXs examined when compared to the T-ALL PDX panel. The light (PDX) to heavy (SILAC) ratio of the JAK1 site pY1034 was the highest in ETP-8 (15-fold) followed by ETP-1 (3-fold) (Fig. 5A). ETP-12 and ETP-13 also had an increased pJAK1 ratio in comparison to the other non-Ph-like PDXs. ETP-ALLs have been reported with mutations in the JAK kinases (10). To confirm that these activating JAK mutations translated from the genomic to the post translational level, the phosphorylation levels of STAT family proteins were investigated. pSTAT5 and pSTAT3 were clearly increased in ETP-ALL PDXs compared to T-ALLs (Fig. 5B). Overall, based on the phosphotyrosine profiling and analysis of pSTAT proteins, it appears that the ETP-ALLs have a higher basal expression of JAK-STAT pathway activation compared to non-ETP T-ALLs despite the fact that not all of the ETPs profiled harbor JAK mutations (Table 1).

The marked up-regulation of the JAK-STAT pathway in the ETP-ALL samples led us to hypothesize that inhibition of this pathway would considerably effect the survival of ETP-ALL PDX cells. We therefore tested the specific JAK1/2 inhibitor ruxolitinib, which is FDA approved for treatment of myeloproliferative diseases (35). Ruxolitinib inhibited JAK signaling by decreasing pSTAT5 and pSTAT3 levels in all ETP-ALL PDXs (Fig. 5B). However in the T-ALL PDXs ALL-8

and ALL-31 elevated levels of pSTAT5 and pSTAT3 were not observed (Fig. 5B). *In vitro* the ETP-ALL samples were marginally more sensitive to ruxolitinib compared to non-ETP T-ALL samples (Fig. 5C). ETP-8, which had the highest ratio of phosphorylated JAK in the profiling study (Fig. 5A), was also the most sensitive to ruxolitinib (IC₅₀ 0.2 μM), followed by ETP-1 (IC₅₀ 0.8 μM) (Fig. 5C). Further, *in vivo* ruxolitinib treatment of the most sensitive ETP-8 PDX resulted in significant reduction of spleen absolute blast counts (p=0.0003) and weights (p<0.0001) compared to the vehicle treated group (Fig. 5D).

While mass spectrometry-based phosphotyrosine profiling is not currently feasible in routine clinical diagnostics, xenografting allows a viable option for this methodology to identify and predict clinically actionable kinase targets for patients who are difficult to treat with conventional therapies. As proof of principle we xenografted a primary refractory BCP-ALL patient biopsy sample (A6199). Although the patient achieved an adequate morphological remission with subsequent rounds of chemotherapy and received a donor transplant, the rising minimal residual disease levels were indicative of incipient ALL relapse. Low resolution genomic analysis was unable to predict any targetable candidates. However, phosphotyrosine profiling of xenografted samples (ALL-77) of this patient revealed elevated levels of LYN kinase phosphorylation (Fig. 6A and Supplementary Table S7). We further validated the upregulation of LYN phosphorylation using immunoblots and compared it to the patient sample along with a SRC kinase activated positive control ALL-4 (Fig. 6B). Although phospho-LYN was detected in the frozen patient bone marrow samples, the levels were considerably higher in the freshly harvested xenografted samples. Furthermore, the exposure of the xenografted cells to dasatinib (1μM, 1h) resulted in complete dephosphorylation of Lyn kinase along with its downstream target phospho ERK (Fig. 6B).

DISCUSSION

Whole genome sequencing and gene expression profiles of aggressive and chemoresistant high-risk subtypes of pediatric ALL have revealed several activating gene fusions, alterations and mutations that could result in constitutively activated TKs (11,12,36,37). In this study, we have developed a quantitative MS-based phosphotyrosine profiling approach compatible with batch mode analysis of proteins obtained from pediatric ALL PDXs to track the global phosphorylation status of TKs. By targeting the activated kinase pathways with commercially available inhibitors, we have also shown that significant *in vivo* responses can be achieved. Overall, this study demonstrates the preclinical utility of our approach and in particular its potential to identify novel, individualized treatments for aggressive and chemorefractory pediatric ALL.

The success of characterizing the tyrosine phosphoproteome in cancer is exemplified by a number of MS-based studies (14,15,18,38). These studies have provided insights into the role of tyrosine phosphorylation in leukemia progression and identified altered TK phosphorylation and novel targets for therapeutic opportunities (39-42). For example, a common phosphotyrosine signature for the BCR-ABL kinase in chronic myeloid leukemia cell lines along with novel fusion kinase signaling and potential drug-responsive biomarkers were identified in one study (23), while in another the changes in T-cell receptor signaling pathways following cisplatin-induced apoptosis were analyzed (40). However, phosphotyrosine profiling studies in leukemias have used cell line models rather than primary patient samples due to the large amounts of protein extract required per experiment.

Even though *in vitro* model systems provide in-depth kinase signaling information, it is very difficult to predict the true effect that any signaling regulation observed would have within a disease microenvironment. To fully understand the relevance and regulation of tyrosine phosphorylation and improve prediction of clinical response after inhibitor treatment, it becomes imperative to study tyrosine phosphorylation in *in vivo* models or directly in patient samples. We recognise that there are significant technical hurdles and challenges for the profiling approach to become a diagnostic clinical tool. One of the key limiting factors being the procurement of large amounts of starting material (peripheral blood/bone marrow) required to profile the relatively low abundance (0.05%) phosphotyrosine molecules (43). However, in the interim, PDX models offer a relevant and feasible

alternative to direct patient samples. We have previously shown that childhood ALL PDXs accurately reflect systemic disease and retain fundamental biological characteristics of the original disease (including responsiveness to treatment) (19,20). The establishment of a quantitative phosphotyrosine profiling method to track the TK signaling changes in a clinically relevant model of ALL is an important step forward.

The regulation of cellular signaling events at a molecular scale by TKs and phosphatases is not only affected by the phosphorylation at selected sites on a given protein but also by their level of phosphorylation. By adopting a decoupled 'spike in' SILAC quantitative methodology (21) in PDX models of pediatric leukemia we were able to successfully integrate this with the phosphotyrosine enrichment protocol. However, we initially observed a preferential capture of heavy SILAC labeled phosphotyrosine peptides when equal amounts of PDX sample and 'spike-in' SILAC standard were used. The likely explanation for this difference is that the xenografted samples had to go through extended processing steps before the cleared mononuclear cells could be lysed or frozen in comparison to cell lines which were directly lysed after a brief wash. It has been well established that processing times in patient samples have an impact on the phosphorylation status due to hypoxia and stress (17). Another possible explanation is that the cell lines receive a pervanadate treatment before cell lysis, in order to retain as many phosphorylated peptides as possible, whereas the PDX samples did not. The percentages of PDX phosphopeptides with a labeled SILAC partner and *vice versa* are shown in Supplementary Fig. S9.

One crucial finding in this analysis was a very high intensity of the Y393 site of TK ABL1 in the ALL-19 (BCP-ALL) PDX along with the classic B-cell signaling non receptor TKs. Y393 is an autophosphorylation site for the ABL1 kinase and is often constitutively activated in BCR-ABL1⁺ ALL patients (23,27). In this study we reconfirmed the phosphorylation of Y393 in ALL-4, which has a *BCR-ABL1* translocation. The identification of active ABL1 in the BCP-ALL PDX (ALL-19) was a unique discovery as there was no previously reported BCR-ABL translocation in this leukemia. Upon further genetic analysis we were able to discover a *NUP214-ABL1* translocation in ALL-19 (unpublished observations). Episomal amplification of *NUP214-ABL1* has been reported in T-cell malignancies and this cell type has also shown sensitivity to dasatinib monotherapy (44,45).

Although the *NUP214-ABL1* translocation is rare in B-cell malignancies, it has been previously reported in Ph-like ALL (12). Moreover, we observed similar sensitivity to dasatinib in ALL-19 *in vivo* indicating the potential of phosphotyrosine profiling to identify activated protein kinases without prior knowledge of kinase translocations and the therapeutic value of the targets. Similarly, the unique upregulation of phosphorylated FLT3 in ALL-2 and the subsequent exome sequencing identification of a novel Y572S mutation highlights the potential of phosphotyrosine profiling to track functional aspects of kinase dysregulation due to point mutations. A similar mutation at site Y572 (Y572 >C) has been reported as a gain-of-function mutation that induced constitutive FLT3 activation. Y572, the first amino acid of the juxtamembrane domain of FLT3, plays a key role in kinase auto inhibition. The crystal structure of the auto inhibited form also reveals that any mutation at this site would result in disruption of its extensive interactions with the surrounding FLT3 subdomains and consequent destabilization of the inactive kinase conformation (46). The increase in phosphorylated FLT3 at known autophosphorylation sites (Y969, Y842) is consistent with high activity of FLT3 (47).

Protein kinase inhibitors represent a possible new treatment option for the chemoresistant ETP-ALL subtype. This high-risk subtype has been reported with high frequency of activating mutations within cytokine receptor and JAK/STAT signaling pathways (10,48). In agreement with the genetic studies, we observed activation of JAK family proteins (JAK1, JAK2, and TYK2) as well as tyrosine phosphorylation of downstream targets STAT5, STAM1 and STAM2A previously reported to be phosphorylated by JAK1-JAK3 (10,49) (Supplementary Table S6). Further, inhibiting the JAK-STAT pathway with ruxolitinib, a specific JAK1/2 inhibitor, clearly demonstrated the reliance of the ETP cells on the JAK/STAT pathway for survival. Taken together, these findings and the previous genetic studies suggest that JAK/STAT pathway hyperactivation may be a hallmark of ETP-ALL and that specific inhibition of this pathway has clear therapeutic relevance, even for those ETP-ALLs without JAK mutation. More recently, we have extended *in vivo* efficacy studies of ruxolitinib to a panel of 6 ETP-ALL PDXs and observed that ruxolitinib demonstrates robust activity irrespective of their JAK mutational status (50).

Deregulation of signaling pathways, whether as a result of fusion, deletion, mutation or amplification of component gene products is a hallmark of high-risk ALL. Targeted inhibition of

perturbed kinases, the key regulators of these signaling pathways, opens novel therapeutic options for high-risk pediatric ALL. Using an unbiased and quantitative tool to identify the tyrosine phosphorylation state of activated kinases in xenograft models of leukemia, we have demonstrated the practical application of this approach in a clinically relevant environment. This study therefore highlights the potential of profiling relapsed and refractory pediatric ALL patients to identify and validate clinically relevant kinases for targeted inhibition with FDA approved drugs in future clinical trials.

ACKNOWLEDGEMENTS

The authors thank the Tissue Resources Core Facility of St Jude Children's Research Hospital (Memphis, TN) for the provision of primary ETP-ALL samples, and the Children's Oncology Group for the provision of the P9906 JAK-mutated primary patient samples. The authors would like to acknowledge Agnes M. Mendo for her assistance in development of the phosphotyrosine enrichment protocol in xenograft models of leukemia. Children's Cancer Institute Australia is affiliated with UNSW Australia and the Sydney Children's Hospitals Network.

REFERENCES

1. Dores GM, Devesa SS, Curtis RE, Linet MS, Morton LM. Acute leukemia incidence and patient survival among children and adults in the United States, 2001-2007. *Blood* 2012;119(1):34-43.
2. Onciu M. Acute lymphoblastic leukemia. *Hematol Oncol Clin North Am* 2009;23(4):655-74.
3. Pui CH, Mullighan CG, Evans WE, Relling MV. Pediatric acute lymphoblastic leukemia: where are we going and how do we get there? *Blood* 2012;120(6):1165-74.
4. Hunger SP, Raetz EA, Loh ML, Mullighan CG. Improving outcomes for high-risk ALL: translating new discoveries into clinical care. *Pediatr Blood Cancer* 2011;56(6):984-93.
5. Moricke A, Reiter A, Zimmermann M, Gadner H, Stanulla M, Dordelmann M, et al. Risk-adjusted therapy of acute lymphoblastic leukemia can decrease treatment burden and improve survival: treatment results of 2169 unselected pediatric and adolescent patients enrolled in the trial ALL-BFM 95. *Blood* 2008;111(9):4477-89.
6. Pui CH, Carroll WL, Meshinchi S, Arceci RJ. Biology, risk stratification, and therapy of pediatric acute leukemias: an update. *J Clin Oncol* 2011;29(5):551-65.
7. Cleaver AL, Beesley AH, Firth MJ, Sturges NC, O'Leary RA, Hunger SP, et al. Gene-based outcome prediction in multiple cohorts of pediatric T-cell acute lymphoblastic leukemia: a Children's Oncology Group study. *Mol Cancer* 2010;9:105.
8. Yeoh EJ, Ross ME, Shurtleff SA, Williams WK, Patel D, Mahfouz R, et al. Classification, subtype discovery, and prediction of outcome in pediatric acute lymphoblastic leukemia by gene expression profiling. *Cancer Cell* 2002;1(2):133-43.
9. Ma M, Wang X, Tang J, Xue H, Chen J, Pan C, et al. Early T-cell precursor leukemia: a subtype of high risk childhood acute lymphoblastic leukemia. *Front Med* 2012;6(4):416-20.
10. Zhang J, Ding L, Holmfeldt L, Wu G, Heatley SL, Payne-Turner D, et al. The genetic basis of early T-cell precursor acute lymphoblastic leukaemia. *Nature* 2012;481(7380):157-63.
11. Zhang J, Mullighan CG, Harvey RC, Wu G, Chen X, Edmonson M, et al. Key pathways are frequently mutated in high-risk childhood acute lymphoblastic leukemia: a report from the Children's Oncology Group. *Blood* 2011;118(11):3080-7.

12. Roberts KG, Morin RD, Zhang J, Hirst M, Zhao Y, Su X, et al. Genetic alterations activating kinase and cytokine receptor signaling in high-risk acute lymphoblastic leukemia. *Cancer Cell* 2012;22(2):153-66.
13. Salomon AR, Ficarro SB, Brill LM, Brinker A, Phung QT, Ericson C, et al. Profiling of tyrosine phosphorylation pathways in human cells using mass spectrometry. *Proc Natl Acad Sci U S A* 2003;100(2):443-8.
14. Rush J, Moritz A, Lee KA, Guo A, Goss VL, Spek EJ, et al. Immunoaffinity profiling of tyrosine phosphorylation in cancer cells. *Nat Biotechnol* 2005;23(1):94-101.
15. Rikova K, Guo A, Zeng Q, Possemato A, Yu J, Haack H, et al. Global survey of phosphotyrosine signaling identifies oncogenic kinases in lung cancer. *Cell* 2007;131(6):1190-203.
16. Wang H, Kadlecck TA, Au-Yeung BB, Goodfellow HE, Hsu LY, Freedman TS, et al. ZAP-70: an essential kinase in T-cell signaling. *Cold Spring Harb Perspect Biol* 2010;2(5):a002279.
17. Baker AF, Dragovich T, Ihle NT, Williams R, Fenoglio-Preiser C, Powis G. Stability of phosphoprotein as a biological marker of tumor signaling. *Clin Cancer Res* 2005;11(12):4338-40.
18. Hochgrafe F, Zhang L, O'Toole SA, Browne BC, Pinese M, Porta Cubas A, et al. Tyrosine phosphorylation profiling reveals the signaling network characteristics of Basal breast cancer cells. *Cancer Res* 2010;70(22):9391-401.
19. Lock RB, Liem N, Farnsworth ML, Milross CG, Xue C, Tajbakhsh M, et al. The nonobese diabetic/severe combined immunodeficient (NOD/SCID) mouse model of childhood acute lymphoblastic leukemia reveals intrinsic differences in biologic characteristics at diagnosis and relapse. *Blood* 2002;99(11):4100-8.
20. Liem NL, Papa RA, Milross CG, Schmid MA, Tajbakhsh M, Choi S, et al. Characterization of childhood acute lymphoblastic leukemia xenograft models for the preclinical evaluation of new therapies. *Blood* 2004;103(10):3905-14.
21. Monetti M, Nagaraj N, Sharma K, Mann M. Large-scale phosphosite quantification in tissues by a spike-in SILAC method. *Nat Methods* 2011;8(8):655-8.
22. Zhang G, Neubert TA. Use of stable isotope labeling by amino acids in cell culture (SILAC) for phosphotyrosine protein identification and quantitation. *Methods Mol Biol* 2009;527:79-92, xi.

23. Goss VL, Lee KA, Moritz A, Nardone J, Spek EJ, MacNeill J, et al. A common phosphotyrosine signature for the Bcr-Abl kinase. *Blood* 2006;107(12):4888-97.
24. Thingholm TE, Jorgensen TJ, Jensen ON, Larsen MR. Highly selective enrichment of phosphorylated peptides using titanium dioxide. *Nat Protoc* 2006;1(4):1929-35.
25. Cox J, Matic I, Hilger M, Nagaraj N, Selbach M, Olsen JV, et al. A practical guide to the MaxQuant computational platform for SILAC-based quantitative proteomics. *Nat Protoc* 2009;4(5):698-705.
26. Cox J, Neuhauser N, Michalski A, Scheltema RA, Olsen JV, Mann M. Andromeda: a peptide search engine integrated into the MaxQuant environment. *J Proteome Res* 2011;10(4):1794-805.
27. Brownlie RJ, Zamoyska R. T cell receptor signalling networks: branched, diversified and bounded. *Nat Rev Immunol* 2013;13(4):257-69.
28. Geiger T, Cox J, Ostasiewicz P, Wisniewski JR, Mann M. Super-SILAC mix for quantitative proteomics of human tumor tissue. *Nat Methods* 2010;7(5):383-5.
29. Gajadhar AS, Johnson H, Slebos RJ, Shaddox K, Wiles K, Washington MK, et al. Phosphotyrosine signaling analysis in human tumors is confounded by systemic ischemia-driven artifacts and intra-specimen heterogeneity. *Cancer Res* 2015;75(7):1495-503.
30. Watts JD, Affolter M, Krebs DL, Wange RL, Samelson LE, Aebersold R. Identification by electrospray ionization mass spectrometry of the sites of tyrosine phosphorylation induced in activated Jurkat T cells on the protein tyrosine kinase ZAP-70. *J Biol Chem* 1994;269(47):29520-9.
31. Newman JD, Harrison LC, Eckardt GS, Jack I. Enhanced insulin-receptor tyrosine kinase activity associated with chromosomal translocation (1;19) in a pre-B-cell leukemia line. *Int J Cancer* 1992;50(3):500-4.
32. Razumovskaya E, Masson K, Khan R, Bengtsson S, Ronnstrand L. Oncogenic Flt3 receptors display different specificity and kinetics of autophosphorylation. *Exp Hematol* 2009;37(8):979-89.
33. Kolb EA, Gorlick R, Houghton PJ, Morton CL, Lock RB, Tajbakhsh M, et al. Initial testing of dasatinib by the pediatric preclinical testing program. *Pediatr Blood Cancer* 2008;50(6):1198-206.

34. Maris JM, Courtright J, Houghton PJ, Morton CL, Kolb EA, Lock R, et al. Initial testing (stage 1) of sunitinib by the pediatric preclinical testing program. *Pediatr Blood Cancer* 2008;51(1):42-8.
35. Verstovsek S. Ruxolitinib: an oral Janus kinase 1 and Janus kinase 2 inhibitor in the management of myelofibrosis. *Postgrad Med* 2013;125(1):128-35.
36. Scheijen B, Griffin JD. Tyrosine kinase oncogenes in normal hematopoiesis and hematological disease. *Oncogene* 2002;21(21):3314-33.
37. Harvey RC, Mullighan CG, Wang X, Dobbin KK, Davidson GS, Bedrick EJ, et al. Identification of novel cluster groups in pediatric high-risk B-precursor acute lymphoblastic leukemia with gene expression profiling: correlation with genome-wide DNA copy number alterations, clinical characteristics, and outcome. *Blood* 2010;116(23):4874-84.
38. Harsha HC, Pandey A. Phosphoproteomics in cancer. *Mol Oncol* 2010;4(6):482-95.
39. Gu TL, Nardone J, Wang Y, Loriaux M, Villen J, Beausoleil S, et al. Survey of activated FLT3 signaling in leukemia. *PLoS ONE* 2011;6(4):e19169.
40. Storvold GL, Landskron J, Strozynski M, Arntzen MO, Koehler CJ, Kalland ME, et al. Quantitative profiling of tyrosine phosphorylation revealed changes in the activity of the T cell receptor signaling pathway upon cisplatin-induced apoptosis. *J Proteomics* 2013;91:344-57.
41. Rubbi L, Titz B, Brown L, Galvan E, Komisopoulou E, Chen SS, et al. Global phosphoproteomics reveals crosstalk between Bcr-Abl and negative feedback mechanisms controlling Src signaling. *Sci Signal* 2011;4(166):ra18.
42. Preisinger C, Schwarz JP, Bleijerveld OB, Corradini E, Muller PJ, Anderson KI, et al. Imatinib-dependent tyrosine phosphorylation profiling of Bcr-Abl-positive chronic myeloid leukemia cells. *Leukemia* 2013;27(3):743-6.
43. Hunter T, Sefton BM. Transforming gene product of Rous sarcoma virus phosphorylates tyrosine. *Proc Natl Acad Sci U S A* 1980;77(3):1311-5.
44. Deenik W, Beverloo HB, van der Poel-van de Luytgaarde SC, Wattel MM, van Esser JW, Valk PJ, et al. Rapid complete cytogenetic remission after upfront dasatinib monotherapy in a patient with a NUP214-ABL1-positive T-cell acute lymphoblastic leukemia. *Leukemia* 2009;23(3):627-9.

45. Quintas-Cardama A, Tong W, Manshouri T, Vega F, Lennon PA, Cools J, et al. Activity of tyrosine kinase inhibitors against human NUP214-ABL1-positive T cell malignancies. *Leukemia* 2008;22(6):1117-24.
46. Frohling S, Scholl C, Levine RL, Loriaux M, Boggon TJ, Bernard OA, et al. Identification of driver and passenger mutations of FLT3 by high-throughput DNA sequence analysis and functional assessment of candidate alleles. *Cancer Cell* 2007;12(6):501-13.
47. Rocnik JL, Okabe R, Yu JC, Lee BH, Giese N, Schenkein DP, et al. Roles of tyrosine 589 and 591 in STAT5 activation and transformation mediated by FLT3-ITD. *Blood* 2006;108(4):1339-45.
48. Neumann M, Heesch S, Schlee C, Schwartz S, Gokbuget N, Hoelzer D, et al. Whole-exome sequencing in adult ETP-ALL reveals a high rate of DNMT3A mutations. *Blood* 2013;121(23):4749-52.
49. Rawlings JS, Rosler KM, Harrison DA. The JAK/STAT signaling pathway. *J Cell Sci* 2004;117(Pt 8):1281-3.
50. Maude SL, Dolai S, Delgado-Martin C, Vincent T, Robbins A, Selvanathan A, et al. Efficacy of JAK/STAT pathway inhibition in murine xenograft models of early T-cell precursor (ETP) acute lymphoblastic leukemia. *Blood* 2015;125(11):1759-67.

FIGURE LEGENDS

Figure 1. Schematic representation of ‘spike-in’ SILAC quantitative phosphotyrosine profiling method developed for PDX models of pediatric ALL. Mouse spleens with > 95% Human CD45⁺ cells are enriched by Ficoll gradient centrifugation and lysed using 8M urea. The cleared lysates are spiked with SILAC mix prior to reduction, alkylation and trypsin digestion. The purified peptides are then lyophilized and immunoaffinity enriched for tyrosine phosphopeptides using pY-100 antibody bound protein A/G beads. Eluted phosphopeptides are filtered through TiO₂ microcolumns prior to mass spectrometric analysis.

Figure 2. Unsupervised hierarchical clustering of Class I phosphosites in 16 pediatric ALL PDXs. (A) Hierarchical Clustering based on the average normalized ratios (PDX/SILAC) of all quantified tyrosine phosphorylated sites enriched by immunoaffinity profiling in 16 PDXs [ETP-ALL (Green), Ph-like- ALL (Yellow), BCP-ALL (Red) and T-ALL (Blue) subtypes]. (B) Clustering based on the average normalized ratios (PDX/SILAC) of TK tyrosine phosphorylation sites. The colors in the heatmaps represent the relative expression per gene across all samples. Red indicates relative high (PDX/SILAC) ratio and blue indicates relative low ratio.

Figure 3. Targeting altered ABL1 signaling in ALL-4 and ALL-19. (A) Normalized ratios (PDX/SILAC) of ABL1-pY393 across 16 PDXs. (B) Immunoblots showing inhibition of ABL1 signaling in ALL-4 and ALL-19 following exposure to dasatinib (1 μ M for 1 h). (C) *In vitro* sensitivity of PDXs to dasatinib. (D) *In vivo* efficacy of dasatinib (50 mg/kg daily x 5 for 4 weeks by oral gavage) against ALL-4 and ALL-19 PDXs. Y axis, % huCD45⁺ cells in the peripheral blood; X axis, days after treatment initiation. The bar graphs represent the mean plus or minus SD of the % huCD45⁺ cells in vehicle treated (Black) or dasatinib (Red).

Figure 4. Targeting altered FLT3 signaling in ALL-2. (A) Normalized ratios (PDX/SILAC) of FLT3-pY842 across 16 PDXs. (B) Normalized ratios (PDX/SILAC) of FLT3-pY969 across 16 PDXs. (C) Immunoblots showing inhibition of FLT3 signaling in ALL-2 following exposure to sunitinib (1 μ M for 1 h). (D) *In vivo* efficacy of sunitinib (53.5 mg/kg daily x 28 days by oral gavage) against ALL-2 PDX. Y axis, % huCD45⁺ cells in the peripheral blood; X axis, days after treatment

initiation. The bar graphs represent the mean plus or minus SD of the % huCD45⁺ cells in vehicle treated (Black) or sunitinib (Red).

Figure 5. Targeting altered JAK1 signaling in ETP-ALL. (A) Normalized ratios (PDX/SILAC) of JAK1-pY1034/1035 across 16 PDXs. (B) Inhibition of JAK/STAT signaling in 6 PDXs following exposure to ruxolitinib (1 μ M for 1 h). (C) *In vitro* sensitivity of ETP-ALL and T-ALL PDXs to ruxolitinib. (D) *In vivo* sensitivity of PDX ETP-8 to ruxolitinib. Graphed are mean plus or minus SD of the spleen absolute blast counts and weights at sacrifice (3weeks) for vehicle and ruxolitinib treated mice. Ruxolitinib (INCB018424) was administered orally as chow formulation for the entire 3 week treatment period.

Figure 6. Elevated LYN phosphorylation and Dasatinib sensitivity in patient sample. (A) Pie chart shows the levels of identified tyrosine phosphorylated peptides of TKs in ALL-77 PDX that was established from the patient (A6199) currently in the clinic. (B) Immunoblots showing inhibition of pLYN and its downstream target pERK in ALL-77 following exposure to dasatinib (1 μ M for 1 h). A6199 lane shows the phosphorylation levels in the patient sample and ALL-4 is used as a positive control.

Table 1. Clinical and molecular features of the patient derived xenograft panel

	Xenograft	Age at Diagnosis (years)	Sex	ALL Subtype	Cytogenetics	Disease Status at Biopsy	Molecular Lesions
B-ALL	ALL-2	5.5	F	BCP	Normal	Relapse	CREBBP D1481H; EP300 Q2268del; FLT3 Y572S; MAPK8IP3 D789N; NT5C2 R238W; NTRK1 G18E; ZNF746 R31H
	ALL-4	8.9	M	BCP	t(9;22), <i>BCR-ABL1</i>	Diagnosis	BAI1 V536I; BCR E552G; RECQL4 A239V; TMPRSS2 K353M; ZBTB32 P438L
	ALL-7	7.4	M	BCP	t(17;19), <i>E2A-HLF</i>	Diagnosis	No validated mutations
	ALL-17	8.11	F	BCP	Normal	Diagnosis	ALG8 R41Q; EPHA5 S810G; FANCF P117T; MLH1 Q460K; MYO3A R1495Q; NRAS G12D; RECQL4 R872K; RUNX1 Q370R
	ALL-19	16.2	M	BCP	Normal	Relapse	CSMD3 H2714fs; CXCR4 F342fs; FAT1 V295M; KRAS L23R; NUP214 N1404fs
Ph-like-ALL	PAKHZT	13.9	M	Ph-like	NA	Diagnosis	JAK2 R867Q; IGH@-CRLF2; CDKN2A/B del
	PALLSD	NA	M	Ph-like	NA	Diagnosis	JAK2 R683G; IGH@-CRLF2; IKZF1del; PAX5del, CDKN2A del
	PAMDRM	7.9	M	Ph-like	46,XY	Diagnosis	JAK2 GPin1682; IGH@-CRLF2; IKZF1del; EBF1del; PAX5 V319fs; CDKN2A/Bdel
T-ALL	ALL-8	12.8	M	T	Normal	Relapse	ALK E1435del; ASXL1 D863G; BRCA2 C1290Y; C3orf35 A29T; EPHA7 K941Q; FBXW7 R465C; KDM6A A30T; NT5C2 R367Q; SCN5A R481W; SMARCA4 R1189Q
	ALL-27	8.6	M	T	Normal	Diagnosis	CREBBP S1934P; FBXW7 R479Q; NOTCH1 L1678P; PIK3CD C416R; RBM28 Y363F
	ALL-29	4.9	M	T	Normal	Diagnosis	BAI1 Q440R; BCL11B G34fs; EPHB3 A498T; FAT1 G855R; JAK1 M206K; NOTCH1 P2514fs; NOTCH1 R1598P; PIK3R5 G612S; SMYD1 A107E
	ALL-31	10.2	M	T	46,XY,del(6)(q21),del(11)(q23)[4]/46,XY[14]	Diagnosis	FBXW7 15_16TR>TLR; HUS1 R33H; LIPM T336N; PTEN NSGPTRRED228fs
	ALL-42	2.7	M	T	Normal	Diagnosis	NA
ETP-ALL	ETP-12	16	M	ETP	NA	Diagnosis	EZH2 S651L; RUNX1 T148fs; NOTCH1 S2492*; IKZF1 SV; PHF6 N147fs; SUZ12 C350R; WT1 C350R L564_S568; SH2B3 SV
	ETP-13	3	M	ETP	NA	Diagnosis	EED S259F
	ETP-1	8	M	ETP	NA	Diagnosis	DNM2 K557_K558>K; JAK3 M511I; WT1R370fs; CTCF SV
	ETP-8	19	F	ETP	NA	Diagnosis	ECT2L E12_splice and W440G; GATA3 A310_A314>A, R276Q; JAK1 E1012>EK; SH2B3 V65A, I257T

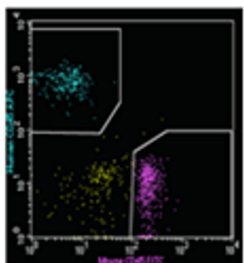
NA, not available; M, male; F, female; m, mutation; del, deletion; SV, structural variation; fs, frame shift. Molecular lesions were identified using exome sequencing for the BCP-ALL and T-ALL groups. Ph-like and ETP-ALL molecular lesions were previously reported (Roberts et al. 2012 and Maude et al. 2015 respectively)

Figure 1

Mononuclear cells
from childhood ALL
BM or PB biopsies

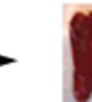


Human CD45+

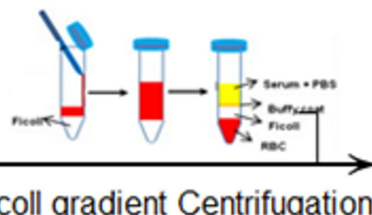


Mouse CD45+

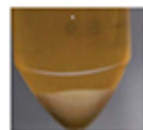
Mouse Spleen



>95%
Human CD45+

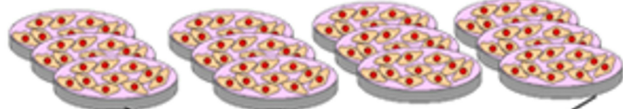


Ficoll gradient Centrifugation



8M Urea
Na3VO4

Jurkat NALM-6 MUTZ-5 MHH-CALL4



SILAC MIX
1:1:1:1

SILAC Spike in

Cell Lysate

Reduction; Alkylation

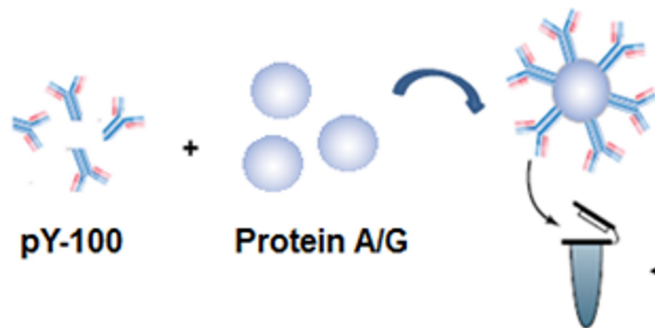
Trypsin Digestion

Desalting (Sep-Pak)

Lyophilise

pY-100

Protein A/G



Phosphopeptide
enrichment (TiO2)

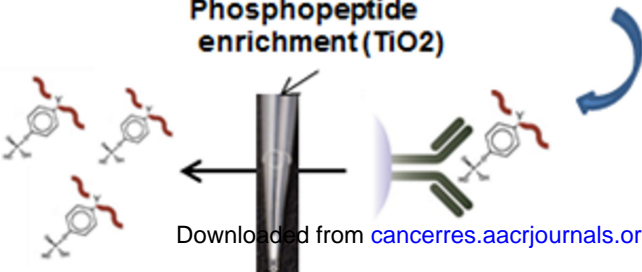
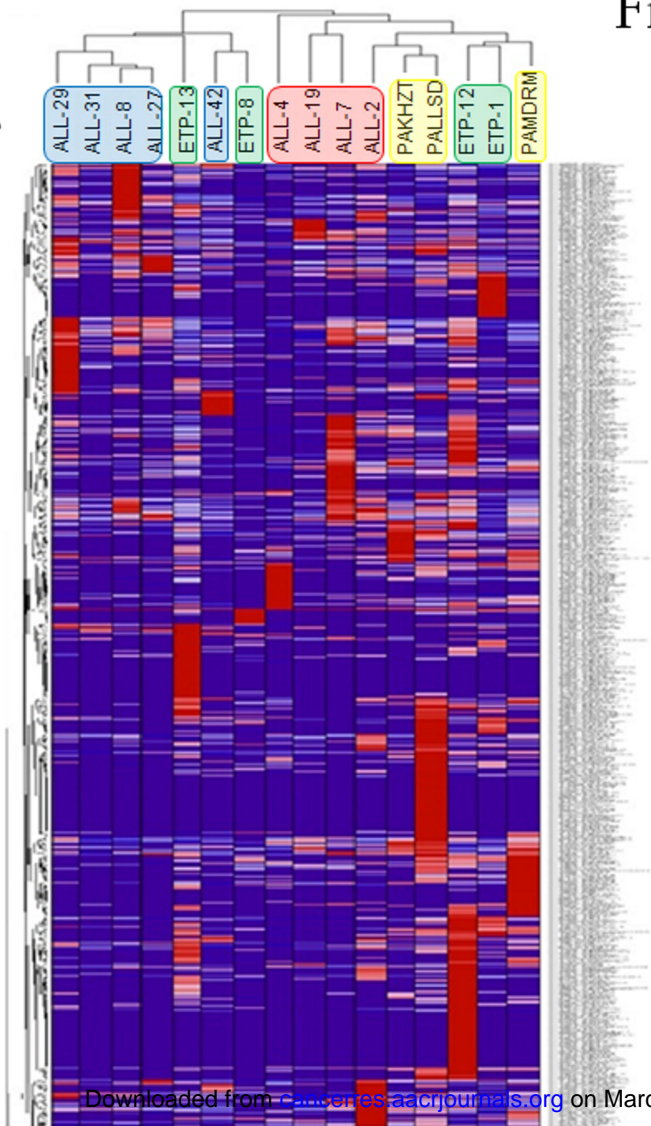


Figure 2

A



B

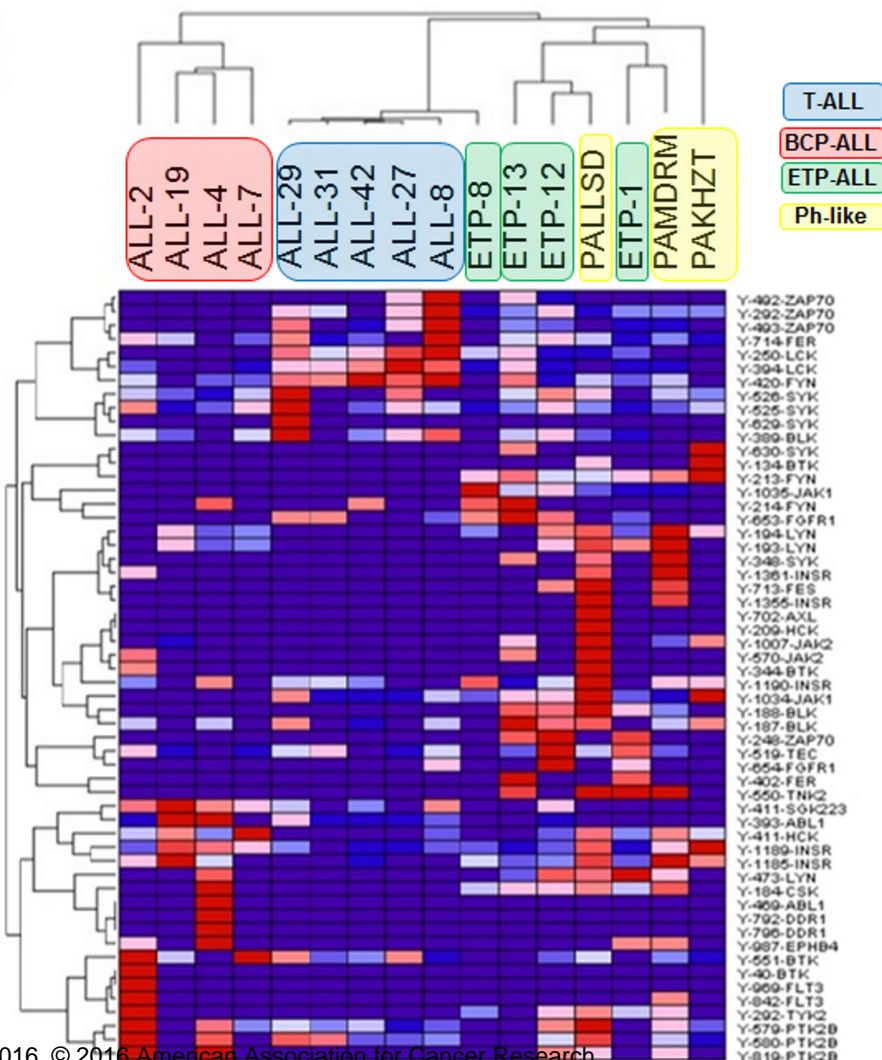


Figure 3

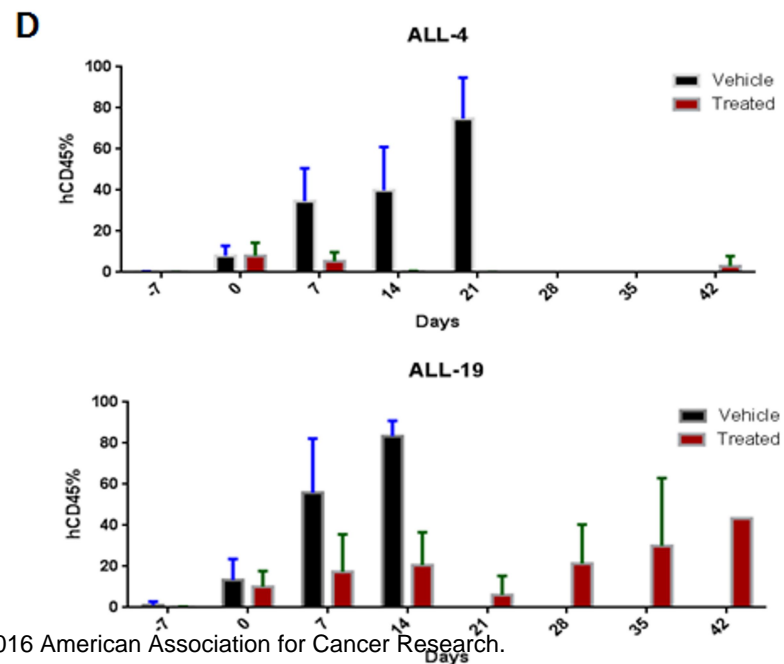
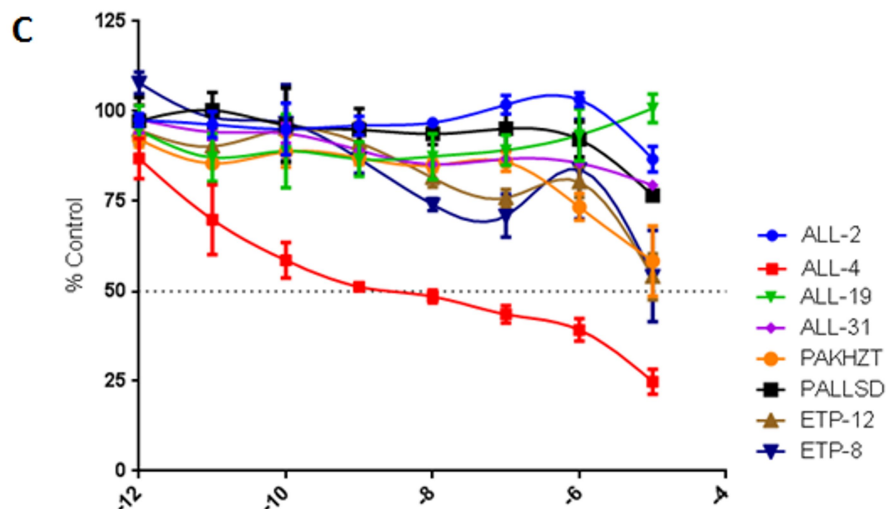
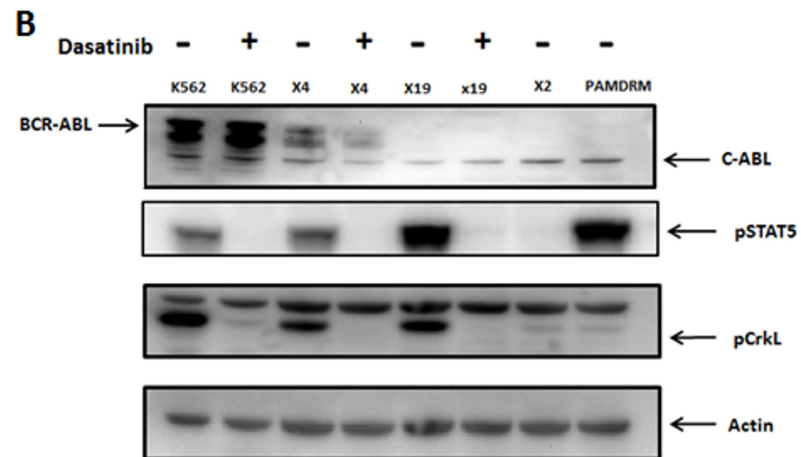
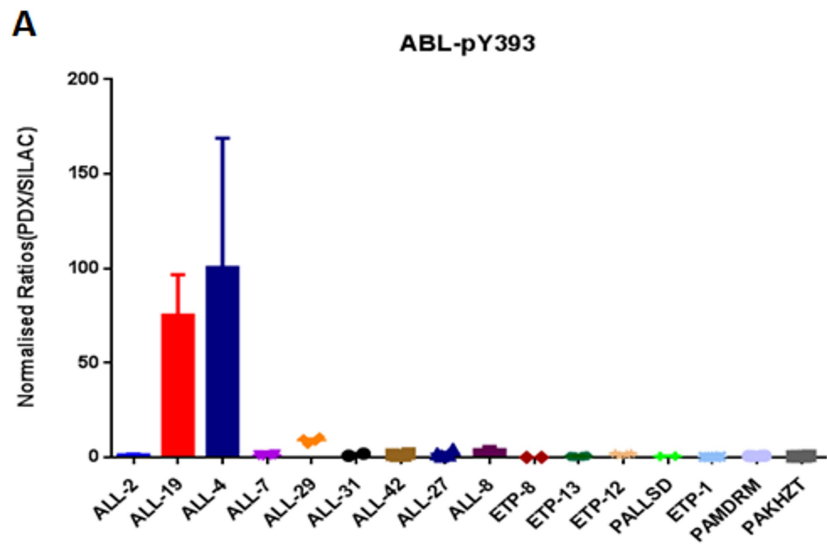


Figure 4

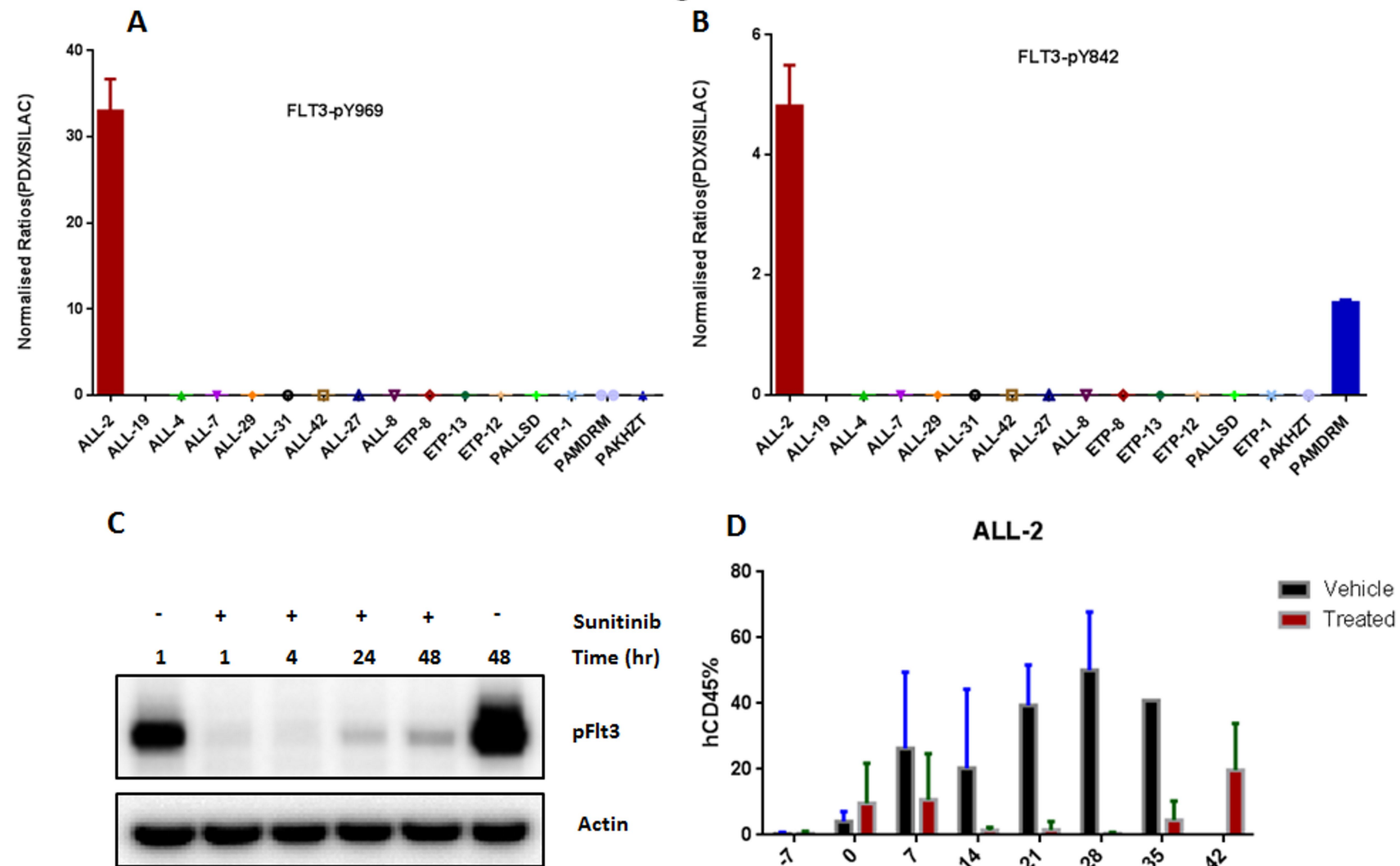


Figure 5

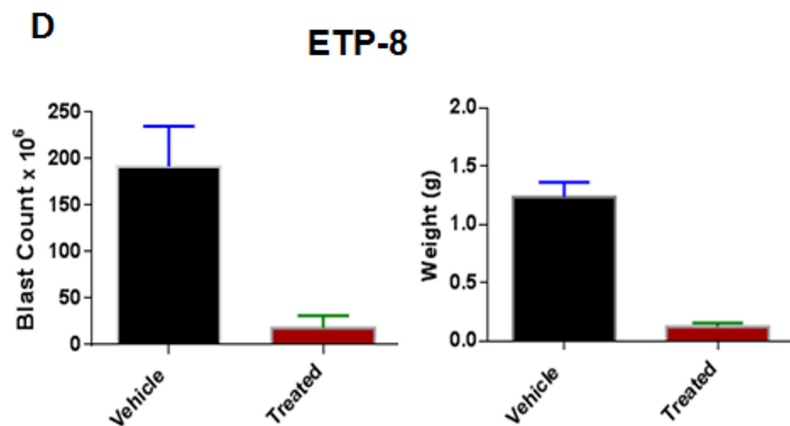
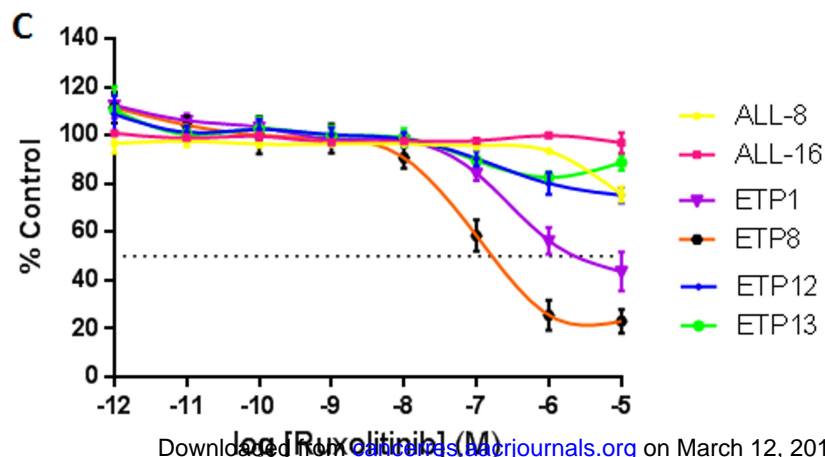
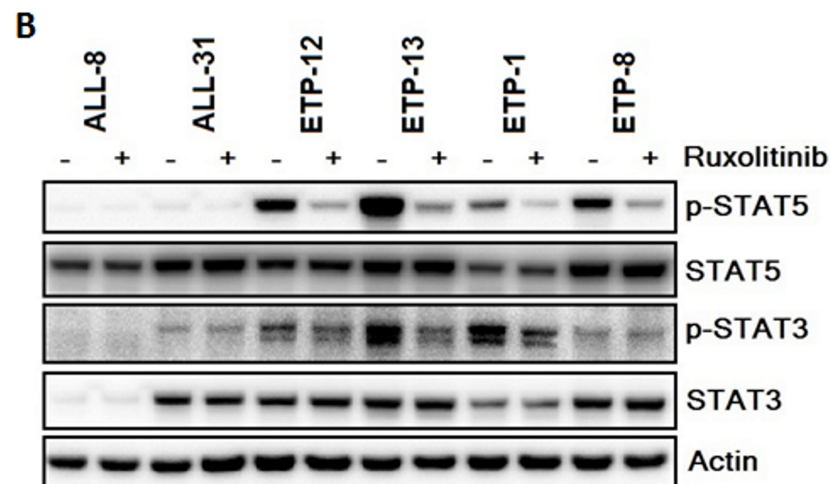
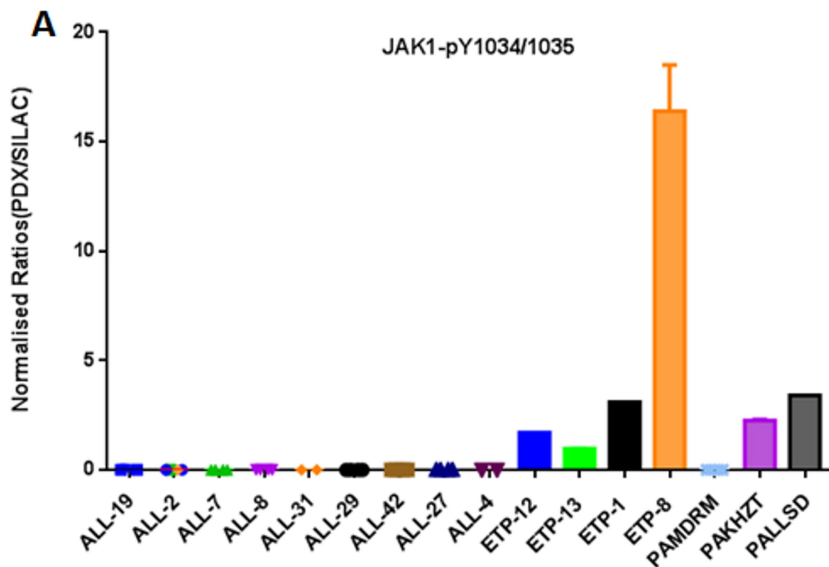
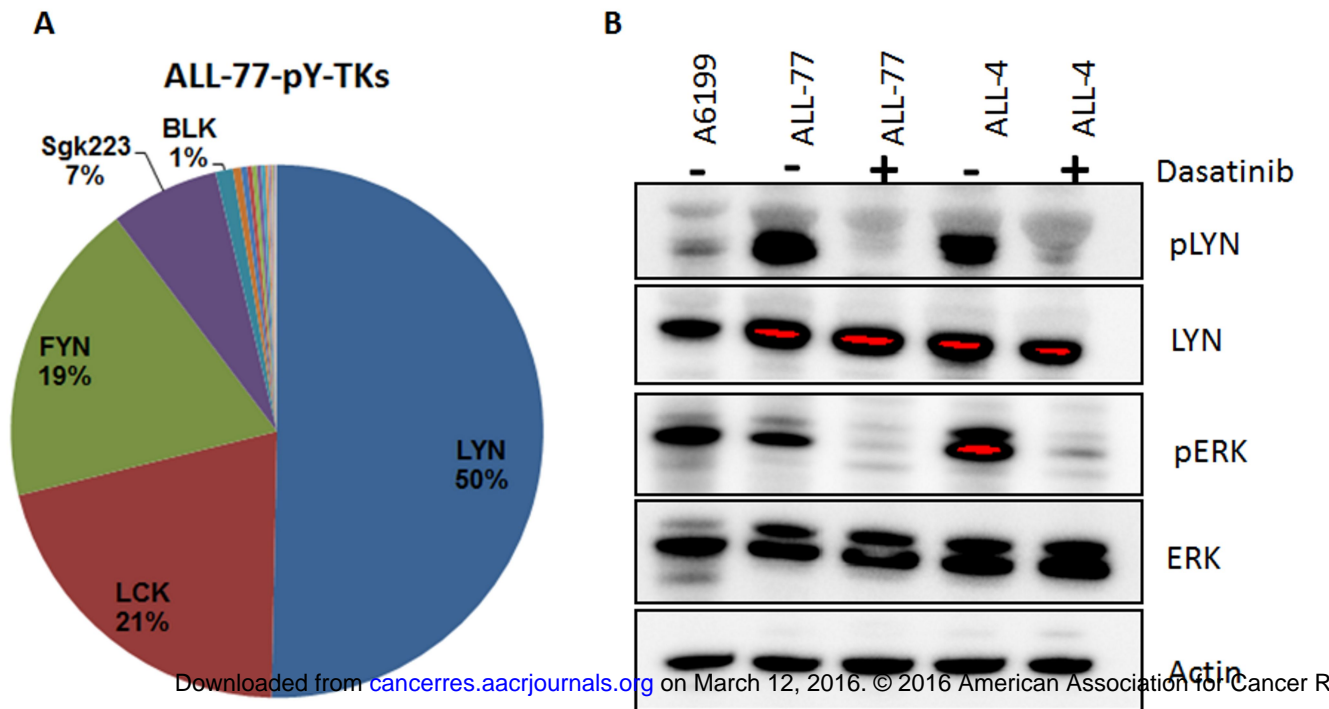


Figure 6



Cancer Research

The Journal of Cancer Research (1916–1930) | The American Journal of Cancer (1931–1940)

Quantitative phosphotyrosine profiling of patient-derived xenografts identifies therapeutic targets in pediatric leukemia

Sibasish Dolai, Keith C. S. Sia, Alissa K. Robbins, et al.

Cancer Res Published OnlineFirst March 9, 2016.

Updated version	Access the most recent version of this article at: doi: 10.1158/0008-5472.CAN-15-2786
Supplementary Material	Access the most recent supplemental material at: http://cancerres.aacrjournals.org/content/suppl/2016/03/09/0008-5472.CAN-15-2786.DC1.html
Author Manuscript	Author manuscripts have been peer reviewed and accepted for publication but have not yet been edited.

E-mail alerts [Sign up to receive free email-alerts](#) related to this article or journal.

Reprints and Subscriptions To order reprints of this article or to subscribe to the journal, contact the AACR Publications Department at pubs@aacr.org.

Permissions To request permission to re-use all or part of this article, contact the AACR Publications Department at permissions@aacr.org.